Turbulent transport regimes and the scrape-off layer heat flux width

J. R. Myra, D. A. D'Ippolito and D. A. Russell

Lodestar Research Corporation, Boulder, CO, USA

Jan. 2015, rev. Mar. 2015

submitted to *Physics of Plasmas*

DOE-ER/54392-76 LRC-15-160

LODESTAR RESEARCH CORPORATION

2400 Central Avenue

Boulder, Colorado 80301

Turbulent transport regimes and the scrape-off layer heat flux width

J. R. Myra, D. A. D'Ippolito and D. A. Russell

Lodestar Research Corporation, Boulder, Colorado, USA

Abstract

Understanding the responsible mechanisms and resulting scaling of the scrape-off layer (SOL) heat flux width is important for predicting viable operating regimes in future tokamaks, and for seeking possible mitigation schemes. In this paper, we present a qualitative and conceptual framework for understanding various regimes of edge/SOL turbulence and the role of turbulent transport as the mechanism for establishing the SOL heat flux width. Relevant considerations include the type and spectral characteristics of underlying instabilities, the location of the gradient drive relative to the SOL, the nonlinear saturation mechanism, and the parallel heat transport regime. We find a heat flux width scaling with major radius R that is generally positive, consistent with previous findings [J. W. Connor et al., Nucl. Fusion **39**, 169 (1999)]. The possible relationship of turbulence mechanisms to the neoclassical orbit width or heuristic drift mechanism in core energy confinement regimes known as low (L) mode and high (H) mode is considered, together with implications for future experiments.

PACS: 52.55.Fa, 52.55.Rk, 52.35.Ra.
Keywords: tokamaks, power exhaust, edge turbulence

I. Introduction

Handling the exhaust of plasma energy from fusion-relevant magnetic confinement experiments poses an important challenge to the fusion community. In steady state the power leaving the machine across the separatrix must equal the total input plus fusion generated power. As fusion-relevant magnetic confinement experiments mature, the powers involved become large. At the same time there is an economically driven motivation to keep experimental dimensions as small as possible. These factors generally conspire to create the potential of large power fluxes on divertor or other material surfaces, a tendency which is already troublesome for the ITER tokamak,[1-3] and which significantly impacts compact high-power density devices such as spherical tori.

The power density P/A on the load bearing surface is determined both by the net power P and the "wetted" area A. Clever divertor designs[4-7] attempt to maximize A through increasing the number of divertor legs, employing flux expansion in the divertor, moving the divertor to large major radius, and tilting the divertor plates while minimizing P by encouraging divertor detachment and radiation of power by the plasma before it reaches the plates. In the simplest and most severe case where plasma energy flows unimpeded along the field lines to the divertor, the area A is proportional to $2\pi R\,\lambda_q$ (times a flux expansion factor) where λ_q is the radial width of the heat flux channel emerging from the midplane region of the torus and R is the major radius. Radiation in the SOL and divertor to mitigate the plasma heat flux, and turbulent spreading of λ_q in the divertor or divertor legs are both highly desirable.[8] Nevertheless, the midplane λ_q remains a fundamental dimension in the problem and is the main subject of this paper.

It has long been thought that the SOL width is determined by competition between parallel transport (i.e. along the magnetic field B) and cross-field turbulent transport.[9-13] Various theories for edge and SOL instabilities have been proposed and employed to give estimates of turbulent diffusion coefficients. Balancing these estimates against collisional parallel heat flow resulted in a variety of predictions for the SOL width. A great number of these theories were reviewed in the late 1990s in an article by Connor.[13] Interest in this problem has grown in the intervening years. The experimental database is much improved and nonlinear edge-SOL turbulence codes have been applied to the problem. Both have provided additional insights into the underlying physics and have helped to motivate the work described here.

Following the treatment in Ref. 13, here we also balance parallel and perpendicular transport in the SOL to determine the SOL width; however, there are some significant differences in the present approach. In addition to locally-driven turbulent transport, a new type of mechanism, distributed transport (related to turbulence spreading) is considered in our paper.

Also, motivated by theoretical progress in edge turbulence, the treatment which follows explicitly considers the role of mean and Reynold's driven sheared flows in turbulence saturation. Our paper compares these turbulence models with the latest experimental data, in particular the H mode data discussed next. Finally, the turbulence mechanism is contrasted with a recently proposed drift-orbit mechanism, which is described subsequently.

An international experimental effort to characterize λ_q in diverted high-confinement (H) mode discharges was carried out,[14-21] and the resulting database has been analyzed in detail.[22] This database yields a nearly linear inverse dependence on plasma current, i.e. $\lambda_q \propto 1/I_p$ with rather weak dependences on other parameters. While high-performance requires operation in H mode, plasma startup generally passes through an Ohmic or low confinement (L) mode phase which can be wall-limited rather than diverted. Experimental investigations of λ_q and its scaling under these conditions is also available.[19,23-26] A weaker than inverse linear dependence on I_p has been reported for these cases, and other parametric dependences also enter. In general, limited L mode discharges produce broader SOLs with larger λ_q.

Advances in the experimental characterization of the SOL width have been paralleled in the theory and simulation community by progress in understanding edge and SOL turbulence. Many groups worldwide have been involved in this work, over the span of at least several decades. While a comprehensive review of edge turbulence is well beyond the scope of this paper, some examples of relevant work may be found in Refs. 27-37 and references therein. Of particular note in the context of boundary turbulence in divertor geometry are simulations using BOUT,[27-30] an electromagnetic three dimensional fluid turbulence code, which encompasses both the confined edge plasma and the SOL. The studies mentioned in this paragraph were not focused specifically on the SOL width, but they have shed valuable insight on the nature of edge and SOL turbulence, the characterization of transport fluxes, nonlinear saturation mechanisms, etc. which are important background to the material which follows in this paper.

Turning specifically to the modeling of λ_q and its scaling, the earliest attempts at nonlinear simulations of the SOL width used reduced fluid turbulence models, such as those embodied in the ESEL[38] and SOLT[39] codes. These models follow filamentary interchange-type structures in the edge and SOL by time-advancing dynamical equations in the two-dimensional (2D) cross-section perpendicular to B, typically at the outboard midplane. Parallel dynamics are approximated by analytical closures.[40,41] These reduced models were able to qualitatively capture many of the scalings that were observed experimentally, and generally produced SOL widths that were comparable (within a factor of two or so) to experimental measurements.[42-45] More recently, three dimensional fluid turbulence models have been employed to model λ_q for limited L mode plasmas.[46-48] Insights gained from these simulations have enabled some significant advances in understanding the theoretical basis for the scaling of λ_q under these

conditions, and some very favorable comparisons with experiments have been achieved.[46-48] Although an inverse-type of dependence on I_p was obtained in the modeling of selected discharges using the SOLT and ESEL codes,[42,44] none of the 2D or 3D fluid simulation efforts have so far been able to satisfactorily explain the experimentally observed Eich scaling[22] (see following) for $\lambda_q \sim 1/I_p$ in H mode discharges.

In contrast to turbulent transport, an entirely different mechanism which has its origins in the neoclassical ion orbit width has been very successful in explaining the Eich scaling. In order of magnitude, this "heuristic drift" (HD) model[49] produces a width $\lambda_q \sim q\rho_s$ where q is the edge safety factor and ρ_s is the ion sound radius. Given plausible arguments for determining the separatrix temperature, which in any case is weakly dependent on machine parameters, the $q\rho_s$ result gives both a $1/I_p$ scaling and absolute widths close to experimental observations. Particle-in-cell (PIC) simulations designed to capture orbit width effects on the SOL began with the XGC-0 code[50] (for 4D gyro-kinetic torodially symmetric modeling with specified background diffusion coefficients) and already noted an inverse scaling with the poloidal magnetic field[51] Studies are continuing with XGC-1[52] (for 5D gyro-kinetic simulations including turbulence). Recent XGC-1 results[53] are consistent with $\lambda_q \sim q\rho_s$ in present day machines but the competition and/or interaction of turbulence and orbit width effects is not yet clear.

Because both orbit-width and turbulence based theory models seem relevant to experimental observations, a deeper understanding of the theoretical basis is needed, especially for the turbulence mechanism which is inherently complex and regime dependent. The goal of this paper is to construct an overarching qualitative and conceptual framework for understanding edge/SOL turbulence with respect to setting λ_q. As such, throughout the paper the approximate equality sign $\approx$ will frequently be used in conjunction with order of magnitude dimensional arguments. Order-of-unity factors are generally not retained, and numerical accuracy is not implied. The focus is rather on scalings and mechanisms. In Sec II a physical basis for estimates of the SOL width in various regimes is presented. Specific scaling results are presented in Sec. III. With this in hand, in Sec. IV we speculate on the competing roles of turbulent transport and orbit width effects as the mechanism for establishing the SOL heat flux width in present day and future larger major radius machines. Finally, conclusions are summarized in Sec. V.

II. Turbulent SOL width mechanism

A. Basic equations

The starting point for examining turbulence as the mechanism for establishing the SOL width is the steady-state power balance equation in the SOL, namely $\nabla \cdot \mathbf{q} = 0$ where $\mathbf{q}$ is the heat flux. In order of magnitude therefore

$$\lambda_q \approx \frac{q_\perp}{q_\parallel} L_\parallel \tag{1}$$

where $L_\parallel$ is a parallel scale length to be defined subsequently. For the turbulence-driven perpendicular heat flux in the near-separatrix region we estimate

$$q_\perp \approx \left\langle \tilde{v}_x \tilde{p} \right\rangle \tag{2}$$

where <..> is a time and poloidal (y) average, x is the radial direction and, for any quantity h, $\tilde{h}$ represents its perturbation with phase variation in space **x** and time t given by exp(i**k**·**x**–iωt). Here p = nT is the pressure and $\tilde{v}_x$ the turbulent radial velocity. Assuming **E**×**B** turbulent convection (note that any contributions with adiabatic phase $\tilde{p} \propto \tilde{\Phi}$ do not contribute to $q_\perp$)

$$\tilde{p} \approx i\tilde{v}_x \nabla p / \omega \tag{3}$$

and taking the time average $\left\langle \tilde{v}_x \tilde{p} \right\rangle = \mathrm{Re}[\, \tilde{v}_x \tilde{p}^* \,]/2$ one obtains

$$q_\perp \approx \frac{\gamma \left\langle \tilde{v}_x^2 \right\rangle p}{|\omega|^2 \lambda_p} \tag{4}$$

Here ω is assumed to be in the plasma drift frame, the radial pressure gradient is $\nabla p \approx p/\lambda_p$ with λ_p the pressure gradient scale length, and $\gamma = \mathrm{Im}(\omega)$ is the instability growth rate. Equation (4) is equivalent to assuming turbulent diffusion, which is plausible for estimation near the separatrix, but known to be a poor description of transport in the far SOL, where blob-filament convection dominates.[40,41] (Nevertheless, in the blob paradigm for curvature driven interchange convection we would estimate $\gamma \sim \omega \sim v_b/\delta_b$ where $v_x \sim v_b$ the blob speed, and $\lambda_p \sim \delta_b$ is the blob radius, so Eq. (4) is still sensible, yielding $q_\perp \sim p v_b$ for the transport of each blob filament.)

A significant caveat in going from Eq. (2) to Eq. (4) is that the given estimate is based on linear phase relationships; however, nonlinear-induced changes in cross-phase between $\tilde{v}_x$ and $\tilde{p}$ in Eq. (2) can influence transport. For interchange modes, where the linear cross-phase maximizes the transport flux, Eq. (4) should be viewed as a reasonable upper limit. Although we will proceed with Eq. (4), an important future task will be investigation of the nonlinear cross-phase and comparison of $1/\gamma$ with the correlation time for the modes responsible for setting the SOL width, using simulations in combination with experimental data.

For the parallel heat flux in Eq. (1) we employ

$$q_\parallel \approx g n T c_s \tag{5}$$

where $c_s = (T_e/m_i)^{1/2}$ is the sound speed, $T \approx T_i \approx T_e$, g is a dimensionless collisionality regime dependent factor, and n and T are midplane values. In the sheath limited regime, where n and T do not vary greatly along a field line, g is the sheath energy transmission factor[54] typically $g \approx 6$, while in the conduction limited (highly collisional) regime $g \approx <3.2\ (m_i/m_e)^{1/2}\ \nu_{te}/(\nu_e L_{||})>_{||}$ where ν_{te} is the electron thermal velocity, ν_e is the electron collision frequency and $L_{||}$ is a parallel scale length which we estimate here, and in Eq. (1), as $L_{||} \approx qR$ where R is the major radius of the torus. In the heuristic expression given for g in the conduction limited regime, $<\ldots>_{||}$ represents an *appropriately weighted* field line average. Note that the variation of n and T, hence collisionality, along the field line can be large in the conduction limited regime. In practice g is often estimated from a two-point model;[54] more accurate evaluation would require a two-dimensional transport code.

Collecting terms, the heat flux width in the SOL can be expressed as

$$\lambda_q \approx \frac{qR\gamma \tilde{v}_x^2}{gc_s|\omega|^2\lambda_p} \tag{6}$$

To make further progress it is necessary to provide specific estimates for the typical instability growth rate γ and frequency ω, and the saturation level $\tilde{v}_x^2$. Additionally the interpretation of λ_q and λ_p requires some discussion.

The major steps, or additional physical inputs, in going beyond Eq. (6) can be categorized as follows:

- types of instabilities
- radial wave-number and eigenfunction scale size
- saturation mechanisms
- types of transport

These will be treated in the sections which follow.

B. Types of instabilities

In this paper, we consider three different types of instabilities which are commonly thought to be relevant to the near-separatrix region: instabilities of the curvature-driven *interchange* type, collisional *drift* wave (DW) instabilities and *flow* instabilities such as Kelvin Helmholtz (KH).

The characteristic growth rate of ideal curvature-driven interchange modes is

$$\gamma_{mhd} \approx \frac{c_s}{(R\lambda_p)^{1/2}} \tag{7}$$

with $|\omega| \approx \gamma$. Of course, by tokamak design, ideal interchange modes are stable on closed field lines, but fast resistive modes, even at modest k values, such as in the case of resistive X-point modes,[27,55] approach this growth rate, and Eq. (7) is also characteristic of the maximum growth rate of interchange modes in the SOL.[56,57] We consider typical wavenumbers k_y for some of these cases next.

The dispersion relation for fast resistive modes (see e.g. Ref. 55 and refs. therein) is given by

$$\frac{\omega\omega_a^2}{\omega + i\omega_\eta} + \omega^2 + \gamma_{mhd}^2 = 0 \tag{8}$$

where $\omega_a^2 = k_\parallel^2 v_a^2 \approx v_a^2 q^2 / R^2$, v_a is the Alfven velocity and $\omega_\eta = \eta_\parallel k_\perp^2 c^2 / 4\pi = 0.51 \nu_e k_\perp^2 \delta_e^2$. Here $\eta_\parallel$ is the Spitzer conductivity, $k_\perp$ and $k_\parallel$ refer to the wavenumber components perpendicular and parallel to the background magnetic field respectively, c is the speed of light, ν_e is the electron Coulomb collision frequency, and $\delta_e = c/\omega_{pe}$ is the electron skin depth. In the strongly resistive limit $\omega_\eta >> \omega$, one estimates $\omega \sim \gamma \sim \gamma_{mhd}$ provided that $\omega_\eta \gamma_{mhd} > \omega_a^2$. The smallest $k_\perp$ for which this is valid is given by

$$k_\eta \equiv \frac{1}{\delta_e} \frac{\omega_a}{(\gamma_{mhd} \nu_e)^{1/2}} \approx \left(\frac{\Omega_e}{\nu_e}\right)^{1/2} \frac{\lambda_p^{1/4}}{qR^{3/4}\rho_s^{1/2}} \tag{9}$$

where $\rho_s = c_s/\Omega_i$. For conventional resistive modes, in limiter (i.e. non-X-point) geometry, this requires large $k_y \sim k_\eta$. In divertor geometry, $k_\perp$ varies strongly along the field lines and is greatly enhanced in the X-point region by magnetic shear. Consequently, fast resistive instability for outer midplane values of $k_y << k_\eta$ is possible. [27,55]

Another characteristic value of k_y arises from considering ion diamagnetic effects. which modify the ω^2 term in Eq. 8 to $\omega(\omega - \omega_{*i})$ where $\omega_{*i} = k_y v_{di}$ and $v_{di} \approx c_s\rho_s/\lambda_p$ is the ion diamagnetic drift velocity. Thus diamagnetic effects modify curvature driven interchange type modes when k_y is of order

$$k_{*i} \approx \gamma_{mhd} / v_{di} \tag{10}$$

Turning now to the electrostatic collisional drift wave, the dispersion relation is (see e.g. Ref. 39 and refs. therein)

$$\frac{i\omega^2 k_\perp^2 \rho_s^2}{\alpha_{dw}} - (1 + k_\perp^2 \rho_s^2)\omega + \omega_{*e} = 0 \tag{11}$$

where $\omega_{*e} = -k_y c_s \rho_s n'/n \approx k_y c_s \rho_s / \lambda_n$ and

$$\alpha_{dw} = \frac{2 k_\parallel^2 v_{te}^2}{\nu_e} \tag{12}$$

When the effective value of $k_{||}$ is specified by geometry so that α_{dw} is given, then the growth rate maximized over $k_\perp$ is

$$\gamma_{dw} \approx \frac{\omega_{*e}^2}{4\alpha_{dw}} \approx \frac{\omega_{*e}^2 \nu_e}{8 k_{||}^2 v_{te}^2} \tag{13}$$

and $\mathrm{Re}(\omega) \approx \omega_{*e}$ provided $\gamma_{dw} << \omega_{*e}$. At peak growth, to within factors of order unity $k_\perp \rho_s \sim 1$.

Finally KH modes can be driven unstable by sheared **E**×**B** flows. KH modes are intrinsically non-local; their growth rate vanishes in the quasi-local limit. A minimal electrostatic model of the KH mode in slab geometry, (see e.g. Ref. 58) results in the eigenvalue equation

$$(\omega - k_y v_y)(\partial_x^2 - k_y^2)\tilde{\Phi} + k_y v_y'' \tilde{\Phi} = 0 \tag{14}$$

where $v_y(x)$ is the prescribed **E**×**B** flow, $v_y' = dv_y/dx$, and $\tilde{\Phi}$ is the perturbed electrostatic potential. In order of magnitude, $\partial_x \sim k_x \sim k_y \sim 1/\lambda_E$, $\omega \sim \gamma \sim v'_{Ey} \approx v_{Ey}/\lambda_E$ where λ_E is the scale length of v_y and the radial electric field. A more careful analysis, using a tanh-type flow profile for $v_y(x)$ shows that at maximum growth $\gamma \sim 0.2\, v_{Ey}/\lambda_E$ and $k_y \lambda_E \sim 0.4$.

C. Radial wave-number and eigenfunction scale size

Assuming that k_y has been chosen to maximize γ, one can then estimate k_x, and the scale size of the radial structure. It is useful to consider three cases for k_y and corresponding estimates for k_x, defined as: *quasi-local* modes with $k_y \lambda_p >> 1$, *non-local* (i.e. "global") modes with $k_y \lambda_p \sim 1$ and *barrier-limited* modes with $k_x \sim \pi/L_x$, which are discussed in detail below. The quasi-local case is of obvious interest for high-k modes such as conventional resistive ballooning modes and collisional drift waves. In the quasi-local regime, one can expand the local growth rate about the point of maximum growth to obtain a parabolic well equation, from which it is found

$$k_x \sim \left(\frac{k_y}{\lambda}\right)^{1/2} << k_y \tag{15}$$

where λ is again the relevant scale length of the driving gradient. The quasi-local regime has been discussed for conventional resistive ballooning modes in Ref. 46, so further details will be omitted here.

In contrast, when $k_y \sim 1/\lambda$, the inequality in Eq. (15) breaks down and the result is a non-local mode with $k_x \sim k_y \sim 1/\lambda$. In steep gradient cases that occur in the edge and SOL, non-local modes are of great importance: frequently there can be no significant separation in scale size between fluctuations that are important for transport and gradient scale lengths.

In SOLT code simulations, it is sometimes found that the radial extent L_x of the dominant non-local modes in the edge and separatrix region is limited to be significantly smaller than that of the driving gradient, i.e. $L_x < \lambda_p$. These are the barrier limited modes referred to earlier. One example is for modes which peak near a point of zero flow shear. Then the flow shear profile can determine the mode's radial scale length. Topology changes at the separatrix as well as magnetic shear effects associated with an X-point can also affect and limit the radial mode structure. Another example occurs for interchange-type modes penetrating into the core region. As the background plasma profiles become less collisional, electron adiabaticity (proportional to α_{dw}) enforces $\tilde{n}/n \approx e\tilde{\Phi}/T$, i.e. the density and electrostatic potential fluctuations are constrained to be in-phase, in contrast to their preferred $\pi/2$ phase relationship from interchange physics. By demanding that $\omega^2 k_\perp^2 \rho_s^2/\alpha_{dw} \sim \omega$ in Eq. (11) and employing Eq. (12) it can be seen that this adiabaticity effect creates a radial barrier for interchange modes when $k_\parallel^2 v_{te}^2/\nu_e > \omega k_\perp^2 \rho_s^2$.

D. Saturation mechanisms

In this paper we consider three different types of saturation mechanisms: wave-breaking (equivalent to pressure gradient modification), sheared flow generation by Reynolds stress, and mean flow suppression.

Wave-breaking occurs when the perturbed flow $\tilde{v}_x$ is just large enough to overtake the phase velocity of the wave.

$$\frac{k_x \tilde{v}_x}{\omega} \approx 1 \tag{16}$$

In most cases, this condition corresponds to pressure gradient modification,[37,39] i.e. the perturbed pressure gradient is comparable to the mean pressure gradient driving the instability

$$k_x \tilde{p} \approx \frac{p}{\lambda_p} \tag{17}$$

The two forms of saturation are equivalent when the pressure perturbation is dominated by **E**×**B** convection, i.e. Eq. (3).

It also turns out the two forms of saturation are equivalent when one considers instabilities of the drift wave type. In that case the pressure perturbation is obtained from an adiabatic relation $\tilde{p} = ne\tilde{\Phi}$. Employing this in Eq. (17) with $\tilde{v}_x = -ik_y\tilde{\Phi}c/B$ expresses the pressure gradient modification condition as $\tilde{v}_x \approx \omega_* / k_x$ where $\omega_* = c_s \rho_s k_y / \lambda_p$. But for drift waves $\omega \sim \omega_*$ so Eq. (17) again reduces to Eq. (16).

The second saturation mechanism is sheared flow generation by Reynolds stress.[59,60] Here we adopt the condition that instability is suppressed when the flow shearing rate exceeds the nominal linear growth rate of the instability.

$$v_y' > \gamma \tag{18}$$

where $' = d/dx = \partial_x$. The sheared flows are generated by Reynolds stress and in steady state balanced by dissipative losses

$$\partial_t v_y + \partial_x \left\langle \tilde{v}_x \tilde{v}_y \right\rangle = -\nu_f \, v_y \tag{19}$$

where ν_f is the flow damping rate. We estimate

$$v_y \approx \frac{\left\langle \tilde{v}_x \tilde{v}_y \right\rangle}{\nu_f \, \lambda_E} \tag{20}$$

where λ_E is the scale length of the resulting v_y flows. Combining with Eq. (18), assuming electrostatic fluctuations with $\tilde{v}_x = -ik_y \tilde{\Phi} c/B$ and $\tilde{v}_y = ik_x \tilde{\Phi} c/B$ the saturation condition for sheared flow generation by Reynolds stress is

$$\frac{k_x \left\langle \tilde{v}_x^2 \right\rangle}{k_y \nu_f \lambda_E^2} \approx \gamma \tag{21}$$

Note that this mechanism causes saturation at a lower amplitude than wave-breaking when $\nu_f \lambda_E^2 k_x k_y < \gamma$. Thus, for non-local modes where $k_x \sim k_y \sim 1/\lambda_E$, i.e. all spatial scales are comparable, the Reynolds mechanism will enter at a lower amplitude than wave-breaking when $\nu_f < \gamma$.

In H mode plasmas, the contemporary paradigm is that instabilities are suppressed by mean flow shear that arises through ion diamagnetic drifts v_{di}.[61-64] We apply Eq. (18) with $v_y = v_{Ey}$ and estimate from the radial force equation that mean **E**×**B** and ion diamagnetic flows balance, $v_{Ey} \approx -v_{diy}$. In order of magnitude, the condition on λ_p to suppress an instability with growth rate γ is $v_{di}' > \gamma$ or

$$\gamma < \frac{c_s \rho_s}{\lambda_p^2} \tag{22}$$

A particular case of interest is that of stabilizing curvature-driven interchange (or fast resistive) modes, for which Eq. (7) applies. Then the condition for H mode-like suppression of transport (i.e. a rough condition for H modes) can be written in the form

$$\lambda_p < R^{1/3}\rho_s^{2/3} \tag{23}$$

E. Types of transport

We assume that transport is ultimately caused by turbulent convection of plasma across the field lines due to the local turbulent **E**×**B** drifts. However, the local **E** can arise either from local instabilities, or in some circumstances from instabilities driven at "remote" locations, e.g. due to a type of turbulence spreading. The sketch in Fig. 1 illustrates the concepts.

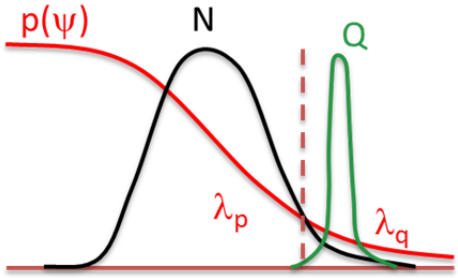

Fig. 1 (color online) Sketch of the radial profiles of the pressure (red), a non-local eigenmode (black, labeled N) and a quasi-local eigenmode (green, labeled Q). The spatial regions for evaluating λ_p and λ_q in the distributed case are as indicated. The vertical dashed line is the separatrix.

For a quasi-local mode in the SOL, the instability is driven by gradients in the SOL which is where we wish to calculate gradients, i.e. to a first approximation we can set $\lambda_p = \lambda_q$. This limit is called *compact*. Quasi-local compact descriptions based on a variety of SOL instabilities characterize most of the SOL width theories.[13,46]

In contrast, a non-local mode can be driven by gradients in the pedestal region but affect transport elsewhere. The mode's associated electric fields extend into the SOL either because of its broad linear radial mode structure, or because of non-linear correlations (e.g. from induced blob propagation or separatrix-spanning convective cells[42]). This case is called *distributed* and we assume that λ_p is given and λ_q is to be calculated. In H mode plasmas, λ_p is assumed to obey Eq. (22).

Several simulations of H mode plasmas using the SOLT code are consistent with the notion of distributed transport as the mechanism for setting the SOL characteristics. An example is shown in Fig. 2 for the simulation of NSTX[65] H mode discharge #138847. The time-averaged pressure profile from the simulation, shown in Fig. 2a), has an inflection point near x = –2cm. The total flow $v = v_{E,y} - v_{di,y}$ is much smaller than $|v_{E,y}|$ or $|v_{di,y}|$ individually; hence, $v_{E,y} \approx -v_{di,y}$ and it follows that there will be a zero in the shearing rate $v_{E,y}'$ near the ion pressure inflection point. In the vicinity of this zero shear point, where $|v_{E,y}'| < \gamma_{mhd}$, curvature driven

modes can create large scale turbulent eddies. These meso-scale structures convect hot plasma $(\tilde{n})$ along contours of Φ from the closed field line region into the SOL, as shown in Figs. 3a) and b). Normalized fluctuations $(\tilde{n}/n)$ in Fig. 3c) show blob structures propagating into the far SOL, as routinely seen experimentally by gas puff imaging.[66] More details of this simulation will be presented elsewhere. For present purposes we note that these simulations employ core particle and heat sources of the type described in Ref. 39. These sources restore the profiles to reference profiles in the core region $\Delta x < 0$, where the separatrix is at $\Delta x = 0$, but are gradually turned off as the separatrix is approached and are strictly zero in the SOL, $\Delta x > 0$. In the SOL, parallel loss terms in the SOLT code provide a physical, albeit reduced-model, description of sink terms. This allows the near separatrix profiles and SOL width to be determined by the turbulent dynamics alone, while imposing a "soft" boundary condition on the core profiles that is chosen to match the measured profiles in a given experiment.

Other recent SOLT simulations[45] of discharges in NSTX provide additional validation of the concept of distributed transport and of the inverse relationship between λ_p and λ_q expressed by Eq. (6). In these simulations, a pre-lithium NSTX discharge with steep pedestal profiles (small λ_p) was compared with a post-lithium discharge where the pedestal profiles were much more gentle (large λ_p). In qualitative agreement with experimental observations, the simulations showed that small λ_p corresponded to larger λ_q, i.e. the midplane SOL width was reduced in the post-lithium discharge. In SOLT, we interpreted the reduced SOL width as resulting from more weakly driven turbulence in the large λ_p case. In this type of simulation, because of the artificial sources discussed in the preceding paragraph, λ_p in the pedestal region is effectively an input, but λ_q in the SOL, being based solely on turbulent transport, is an output. A more complete and predictive treatment would involve turbulence simulations of the entire pedestal region as well as the SOL, but this is beyond the scope of the simulations discussed here.

III. SOL width scaling

A. Scaling examples

Using the basic concepts described in the preceding sections, it is possible to derive scaling laws for λ_q in various regimes. The procedure is best illustrated by considering a specific case.

A suitable example is that of non-local barrier-limited interchange modes, saturated by wave-breaking in the distributed transport case. Starting from Eq. (6) we apply the wave-breaking estimate for $\tilde{v}_x$ given by Eq. (16), take $k_x \sim \pi/L_x$ and employ the curvature-driven interchange growth rate scaling of Eq. (7) to obtain

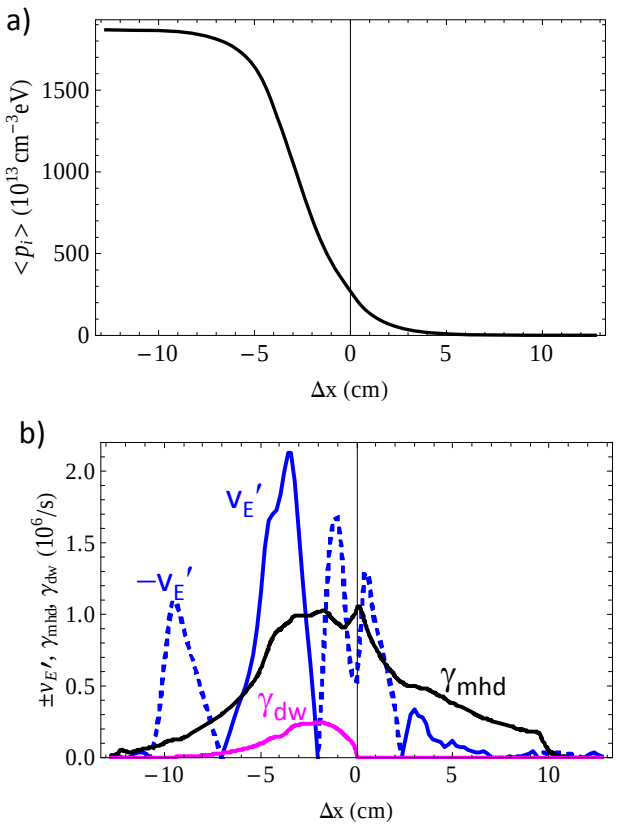

Fig. 2 (color online) SOLT simulation results showing a) the mean ion pressure profile, b) comparison of the ExB shearing rate and the ideal MHD growth rate vs. distance from the separatrix, $\Delta x = 0$. Also indicated is the smaller drift wave growth rate γ_{dw} from Eq. (11) optimized over k_y.

$$\lambda_q \approx \frac{qR^{1/2}L_x^2}{g\pi^2\lambda_p^{3/2}} \tag{24}$$

If the transport regime were changed from distributed to compact, then we would set $\lambda_p = \lambda_q$ and solve for λ_q to obtain

$$\lambda_q \approx \frac{q^{2/5}R^{1/5}L_x^{4/5}}{g^{2/5}\pi^{4/5}} \tag{25}$$

B. Results

An abbreviated notation for the various regimes is given in Table 1. Clearly a large number of combinations are mathematically possible, some more physically interesting than others. In Table 2 the resulting scalings for several different combinations are given.

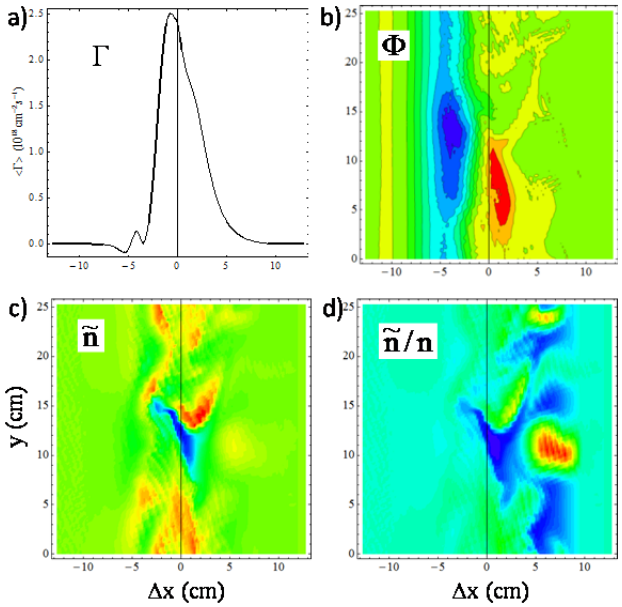

Fig. 3 (color online) SOLT simulation of distributed transport in H mode: a) radial profile of the turbulent particle flux vs. distance from the separatrix, b) contours of electrostatic potential for a snapshot in time, c) density fluctuations and d) normalized density fluctuations at the same time. The separatrix is located at $\Delta x = 0$. Note the decrease in Γ for $\Delta x > 0$ due to SOL parallel losses competing with transport.

Instability	Localization	Saturation	Transport
interchange (I)	quasi-local (Q)	wave-breaking (W)	compact (C)
drift (D)	non-local (N)	Reynolds flows (R)	distributed (D)
flow (F)	barrier (B)	mean flows (M)	

Table 1. Abbreviated notation for the types of instabilities, and the regimes of localization, saturation and transport. One entry is picked from each column, e.g. I-BWD for the example illustrated in the text.

Although no general proof is apparent, it is evident from Table 2 that positive explicit scaling with major radius R (i.e. R to a positive power) is prevalent. The reason may be traced to the $L_{||}$ or qR scaling originally present in Eq. (6) which typically cannot be completely overwhelmed by other factors. For example, the interchange growth rate introduces a weaker

$R^{1/2}$ variation in the denominator leaving a net positive scaling of $R^{1/2}$. In the compact regimes, the λ_p in the denominator is equal to and combined with the λ_q being solved for, which changes the power of the R in the final scaling, but not the fact that the scaling is positive. There is the possibility of implicit R scalings in some of the other quantities; however, the explicit positive R scaling is very significant when considering the extrapolation of mechanisms for λ_q to future large machines.

IV. Discussion

A. SOL width regimes

Full simulations of individual cases for different profiles and parameters would be required to determine the dominant instability and the corresponding relevant scaling law from Table 2. While this is well beyond the scope of the present paper, it is possible to make some speculations about the relationships between several important regimes. A diagram illustrating the concepts is shown in Fig. 4. In the diagram, for illustration, we take the ever-present curvature drive as the instability mechanism.

This diagram has some superficial similarities to Fig. 1 in the paper by Rogers et al.,[31] in that both diagrams consider L and H mode regimes. However, Fig. 4 is not intended to be a predictive diagram for the L-H transition. Rather the intention is only to illustrate the effect of L and H mode parameter regimes on the SOL width, an issue that was not considered in the local flux tube model of Ref. 31. Note that Eqs. (22) and (23), employed here to define the H mode, are consistent with the discussion in Ref. 31 about the role of transport suppression by sheared **E**×**B** flows, arising in the final H mode state from ion pressure in radial force balance. This picture is also consistent with more recent models that consider the dynamics of the L-H transition.[61-64] Finally, the ideal instability boundary is indicated qualitatively in Fig. 4 as a boundary of interest: it may have implications with respect to "stiff" transport (i.e. a critical gradient beyond which transport becomes very large) near the separatrix and also to the density limit. These are topics to which we will return. A somewhat different density limit mechanism and boundary is discussed in Ref. 31.

Starting in the L mode regime, scale lengths such as λ_E are long and mean flow suppression effects are assumed to be negligible, i.e. $v_E' < \gamma_{mhd}$. These cooler plasmas in the vicinity of the separatrix are generally well described by quasi-local resistive instabilities and give rise to a scaling like I-QWC in Table 2. This is because local instability is possible everywhere radially and hence compact transport results. Owing partly to the rather large power of R relative to ρ_s in this scaling, the resulting L mode λ_q is typically rather large, in the several

cm range.[46-48] For these compact modes, $\lambda_q = \lambda_p$ and hence L modes exist below the sheared flow suppression threshold estimate given by Eq. (23).

In H mode plasmas, the steeper gradients implied by Eq. (23) result in sheared flow suppression of the turbulence, and as discussed in Sec. II E, can result in barrier limited modes which exhibit distributed transport. Examples in Table 2 are the I-BRD, I-BWD and F-BWD cases. These scalings typically produce rather smaller $\lambda_q$than their L mode counterparts.

When predicted turbulent SOL widths exceed the HD neoclassical estimate, $q\rho_s$, it is reasonable to assume that turbulence is the dominant mechanism, although a two-scale-length SOL might also be possible in this case.[26,67] In the opposite limit where the turbulence-generated width is less than the ion orbit excursion, $\lambda_q < q\rho_s$ turbulence is likely irrelevant, or at least, its effects must be computed in the context of neoclassical orbit physics. This limits the rightmost extent of the diagram in Fig. 4.

For a given λ_p increasing separatrix pressure will ultimately result in exceeding the ideal MHD stability limit for electromagnetic ballooning modes, $\alpha_{mhd} > \alpha_{crit} \sim 1$, as indicated in the diagram. Resulting turbulence saturation levels are very high and may reasonably be expected to result in destruction of the SOL, i.e. ideal MHD imposes a hard limit beyond which operation is not possible. If this is the case, ideal modes might provide a kind of stiff transport that sets the pressure gradient at a critical value near the separatrix.[68] It is a matter of current debate whether high performance H mode plasmas always operate near the SOL α_{mhd} limit,[69] or only do so when also near the density limit.[70,71] Indeed, Goldston has pointed out that combining the estimate $\lambda_p \approx q\rho_s$ with $\alpha_{mhd} \approx q^2 R 8\pi p/(B^2\lambda_p) \approx 1$ applied at the separatrix results in a scaling that is reminiscent of the Greenwald density limit scaling.[70] Although the detailed arguments are more complex, the basic idea is that the combination of these two scalings gives a limit on the separatrix density

$$n_{sep} \approx \left(\frac{B\rho_s}{8\pi T_{sep}}\right)\left(\frac{B}{qR}\right) \propto \frac{1}{T_{sep}^{1/2}}\frac{I_p}{a^2} \tag{26}$$

The $B\rho_s/8\pi T_{sep}$ factor scales weakly with separatrix temperature, which can be estimated from a SOL power flow model, but in any case is not highly variable, while the $B/(qR) \sim I_p/a^2$ factor is akin to the Greenwald scaling. Taking into account the fact that the Greenwald scaling is for core line density, while the present limit is for separatrix density, it can be shown[70] that the constant of proportionality is also reasonable. Thus, within the accuracy of heuristic arguments, the density and separatrix MHD limits on the separatrix pressure coincide at the right of the diagram in Fig. 4.

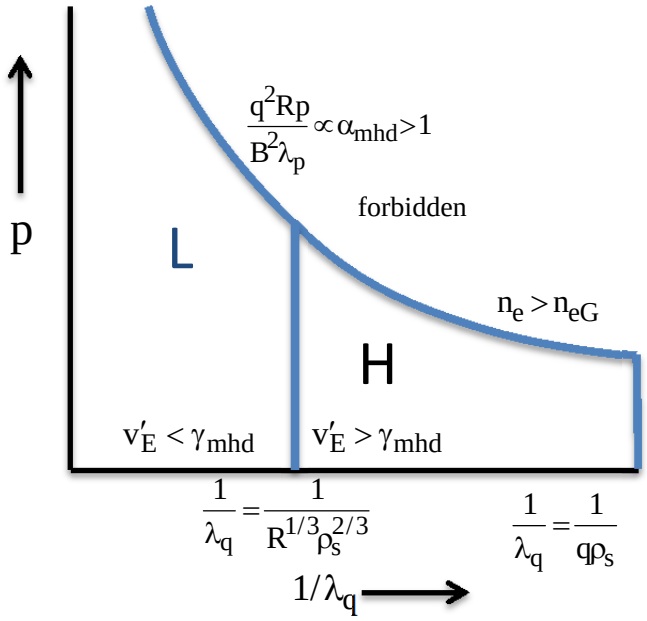

Fig. 4 (color online) Speculative diagram showing the boundaries of L mode and H mode plasmas relative to the separatrix pressure (vertical axis) and inverse SOL heat flux width (horizontal axis).

Key	λ_q scaling	Remarks
I-QWC	$\frac{q^{8/7}}{g^{4/7}}\left(\frac{\nu_e}{\Omega_e}\right)^{2/7} R^{5/7}\rho_s^{2/7}$	Halpern resistive scaling[46]
I-QWC	$\left(\frac{qR\rho_s}{g}\right)^{1/2}$	diamagnetic-modified interchange $\gamma \sim \omega_{*i}$
I-BWC	$\left(\frac{q}{g}\right)^{2/5} R^{1/5}\left(\frac{L_x}{\pi}\right)^{4/5}$	
D-QWC	$\left(\frac{q}{4C_{dw}g}\right)^{1/3} R^{1/3}\rho_s^{2/3}$	C_{dw} = typical $k\rho_s \sim 0.2$ to 1.0
I-NWD	$\frac{q}{g}(\lambda_p R)^{1/2}$	large! even larger if D $\rightarrow$ C
I-BRC	$\lambda_q = \left(\frac{q}{g}\frac{\nu}{\Omega_i}\right)^{1/2}\left(\frac{R}{\rho_s}\right)^{1/2}\frac{L_x}{\pi}$	
I-BWC	$\lambda_q = \left(\frac{q}{g}\right)^{2/5} R^{1/5}\left(\frac{L_x}{\pi}\right)^{4/5}$	
I-BRD	$\frac{q}{g}\frac{\nu_f}{\Omega_i}\frac{RL_x^2}{\pi^2\lambda_p\rho_s}$	$\propto \nu_f/\lambda_p$; independent of γ
I-BWD	$\frac{q}{g}\frac{R^{1/2}L_x^2}{\pi^2\lambda_p^{3/2}}$	upper limit of BRD for $\nu_f \sim \gamma$
F-BWD	$0.2\frac{q}{g}\frac{L_x^2}{\pi^2}\frac{R\rho_s}{\lambda_E^3}$	flow-driven instability
HD	$q\rho_s$	Goldston heuristic drift model (simplified)[49]

Table 2. Scaling results for λ_q in several regime combinations. The last row, a simplified version of the characteristic λ_q for the heuristic drift model is given for comparison with the turbulence based models.

B. Inter-machine scaling

Although "order unity" numerical factors have not generally been retained in the preceding analysis, it is still important to check the reasonableness of the results quantitatively at an order-of-magnitude level. It is also interesting to speculate on the consequences of any trends. In doing so, however, it should be emphasized that, given the heuristic level of estimates in this paper, no claims about absolute accuracy should be inferred.

Order-of-magnitude estimates are presented in Fig. 5 where the I-BWD and F-BWD scaling results from Table 2 are compared with the HD model and with a fit to a multi-machine experimental database due to Eich[22] for the inter-ELM phase of H mode plasmas. We show the comparison with I-BWD and F-BWD for several reasons: the interchange and flow drive mechanisms should be always present in H mode; Sec. II E suggests the barrier limited distributed transport mechanism in H modes; and, wave-breaking saturation gives an upper limit on the cross-field turbulent transport relative to the Reynolds flow mechanism, and hence an upper limit on λ_q. Furthermore, it can be argued[72] that KH turbulence limits the Reynolds-driven sheared flow that stabilizes curvature driven modes. In this picture the I-BWD and F-BWD models provide upper and lower limits for λ_q.

The long-dashed black line in Fig. 5 is the multi-machine scaling. For illustration we employ regression fit #15 in Table 3 of Ref. 22 which includes spherical tori (and hence allows a significant range in ε). This fit takes the explicit form for λ_q at the midplane

$$\lambda_q = 1.35\, P_{SOL}^{-0.02} R^{0.04} B_p^{-0.92} \varepsilon^{0.42} \tag{27}$$

where the units are λ_q(mm), P_{SOL}(MW), R(m), B_p(T) and ε = a/R. This regression fits the measurements in MAST, NSTX, Alcator C-Mod (CMOD), ASDEX-U (AUG), DIII-D, and JET tokamaks to within a factor of two or better. Note that Fig. 5 does not show actual experimental data but rather evaluates Eq. (27) at nominal machine parameters. Recent EAST tokamak measurements[20] (not included in the regression fits of Ref. 22) determined λ_q to be roughly a factor of 2 larger than the multi-machine fits.

Several specialized assumptions have been made in Fig. 5. For the I-BWD and F-BWD points, the pre-factor q/g in Table 2 has been set to unity which is reasonable for order-of-magnitude estimates in a sheath-limited SOL regime. For more collisional conduction limited SOL conditions, the illustrated results should be increased by q/g which may be larger than 1. For the machine parameters, B_t, B_p, a and R we employ representative (approximately midrange) values from Table 1 of Ref. 22. For the EAST tokamak representative parameters are taken from Ref. 20. The ion charge and mass employed in Fig. 5 are that of deuterium. The gyroscale ρ_s is calculated from the total B, using for T_e an estimate of the separatrix temperature given by Eq.

(7) of Ref. 49, which is based on SOL power flow using a two-point model. In fact, the turbulence results are rather insensitive to T_e as can be seen from the explicit scalings. In Fig. 5, no distinction has been made between the radial scale lengths L_x, λ_E, and λ_p; and, λ_p was calculated from the H mode condition given by Eq. (23) (with equality). This gives scale lengths on the order of a cm for most of the machines, and is meant to apply in the pedestal foot, near the separatrix. Finally, for the simplified HD result, we employed the value q = 4 (for q_{95} at the 95% flux surface).

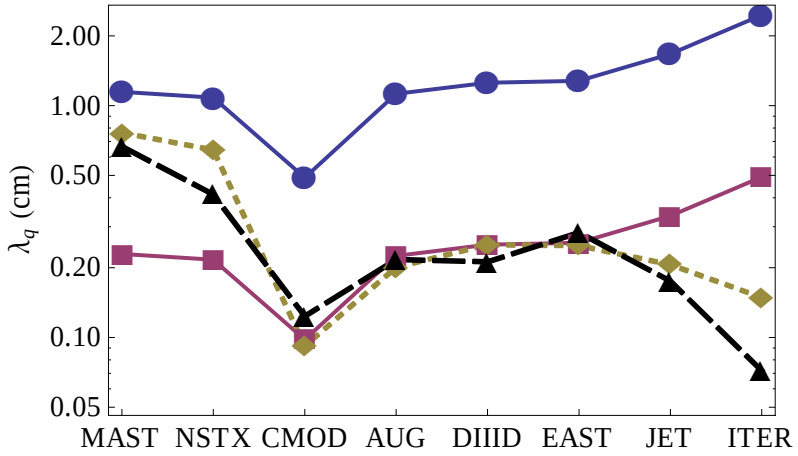

Fig. 5 (color online) Order-of-magnitude estimates for the size of the midplane SOL heat flux width in the indicated machines, resulting from the mechanisms I-BWD (blue), F-BWD (plum), simplified HD (dashed gold), and Eich fit #15 (long-dashed black).

It is reasonable to make several inferences from Fig. 5. First, as is already well known, the HD model (dashed gold curve) even in the simplified form used here, fits existing experiments remarkably well. However, turbulence-based models can also be at least order-of-magnitude consistent with experimental data. Additionally, there is some indication that the turbulence-based models follow broad experimental trends. For example, the pronounced dip in λ_q for Alcator C-Mod is captured by all the models. This is not unexpected because both R and ρ_s are relatively small in C-Mod. Significant differences between the turbulence-based models and the HD model (or the projection of the Eich fit) emerge when applied to ITER. Finally, it is remarkable how closely the F-BWD curve follows the HD and Eich curves for Alcator C-Mod, ASDEX-U, DIII-D and EAST parameters. The level of numerical agreement is almost certainly fortuitous, but the agreement of the trends may be significant, either physically, or at least to suggest co-dependencies in the multi-machine database.

Figure 5 presents evidence for the relevance of turbulence as a SOL broadening mechanism in non-ELMing (or inter-ELM) diverted H mode plasmas. More generally, SOL turbulence broadening can be considered in other regimes, as discussed in the preceding sections. It has already been shown in other work[44,46-48] that resistive interchange or ballooning turbulence (of the I-QWC type) provides a plausible explanation for λ_q in limited L mode discharges. Consequently, similar L mode comparisons need not be repeated here.

V. Conclusions

In summary, we have applied simple heuristic considerations for the turbulent transport flux across the separatrix to obtain regime-dependent analytical scaling laws for the midplane heat flux width λ_q. These are given for various regime combinations in Table 2. These estimates are all based on balancing turbulent perpendicular transport with parallel transport in the SOL. An alternative picture, briefly mentioned in connection with Fig. 4 but not otherwise treated here, is that the SOL width, at least in some regimes, could be set by a critical gradient mechanism, e.g. one which maintains profiles at or near marginal stability to ideal ballooning modes.[69,70]

In our model, the most important factors determining the regime are the instability type, the radial wave-number and eigenfunction scale size, the nonlinear saturation mechanism, and the type of transport process. The collisionality of the SOL, i.e. the parallel transport regime, also directly impacts the final result for λ_q.

The concept of distributed transport was illustrated with some simulation results which distinguish between the radial location and size of the turbulence driving gradient and the SOL responding gradient. The heuristic estimates qualitatively explain some of the SOL width results seen in numerical SOLT code simulations of H mode plasmas, in particular, the inverse scaling of λ_q with λ_p in the distributed transport regime. Thus, the turbulent SOL heat flux width in L mode and H mode plasmas may depend on different transport mechanisms, compact vs. distributed, respectively.

In direct order-of-magnitude comparison with the multi-machine experimental database for the inter-ELM phase of H mode plasmas, sample turbulence mechanisms are order-of-magnitude reasonable, and capture some of the observed trends, as illustrated in Fig. 5. However, none of the investigated turbulence models produces a clean $\lambda_q \propto 1/I_p \propto q\rho_s$ scaling. The HD (neoclassical orbit width) model does give this scaling and explains existing experimental H mode data rather well. It is tempting to speculate that the turbulence mechanism is sub-dominant with the orbit width mechanism, but nevertheless quite possibly present, in the H mode plasmas of today's machines. Further investigations will be required to determine the

nature of possible fundamental interactions between turbulence and finite orbit width effects in the vicinity of the separatrix. One aspect of this is the role turbulence could have on the electron heat channel in the SOL[49] and on ambipolarity in the closed surface region.[71] Evidence presented elsewhere suggests the importance of turbulence broadening of the SOL in limited L mode discharges.[24,25] Significantly, in all the regimes examined here, turbulence mechanisms tend to give λ_q a positive scaling with R and thus can be relatively more dominant in large machines like ITER than the HD model which just depends on ρ_s. If this turns out to be the case, it would be a favorable result for reducing the potentially damaging heat flux impacting the divertor plates.

The primary goal of this paper has been to determine scalings for the SOL width under various assumptions about the physical processes involved, with an emphasis on turbulence as the transport mechanism. In closing, two caveats about interpretation should be emphasized: (i) little significance should be attached to the numerical values of λ_q obtained here (i.e. the scaling prefactors) except their rough order-of-magnitude; (ii) the validity of the derived scalings rests upon an understanding of the underlying processes for instability drive, saturation, etc. and the resulting turbulent transport fluxes, including issues such as the nonlinear cross-phase. This work is still very much ongoing and needs validation by both numerical modeling and direct comparison with experiments. It is hoped that the present work will provide a framework for further developments towards this goal.

Acknowledgments

This material is based upon work supported by the U.S. Department of Energy Office of Science, Office of Fusion Energy Sciences, under Award Number DE-FG02-97ER54392. The authors thank Y. Sechrest and the NSTX Team for providing some of the basic discharge data used in the sample simulation results of Figs. 2 and 3.

References

[1] B. Lipschultz, X. Bonnin, G. Counsell, A. Kallenbach, A. Kukushkin, K. Krieger, A. Leonard, A. Loarte, R. Neu, R.A. Pitts, T. Rognlien, et al., Nucl. Fusion **47**, 1189 (2007).

[2] A. Loarte, B. Lipschultz, A.S. Kukushkin, G.F. Matthews, P.C. Stangeby, N. Asakura, G.F. Counsell, G. Federici, A. Kallenbach, K. Krieger, et al., *Progress in the ITER Physics Basis, Chapter 4: Power and particle control*, Nucl. Fusion **47**, S203 (2007).

[3] A. Herrmann, Plasma Phys. Control. Fusion **44**, 883 (2002).

[4] D. D. Ryutov, Phys. Plasmas **14**, 064502 (2007).

[5] M. V. Umansky, R. H. Bulmer, R. H. Cohen, T. D. Rognlien, and D. D. Ryutov, Nucl. Fusion **49**, 075005 (2009).

[6] P. M. Valanju, M. Kotschenreuther, S. M. Mahajan, and J. Canik, Phys. Plasmas **16**, 056110 (2009).

[7] M. Kotschenreuther, P. Valanju, B. Covele, and S. Mahajan, Phys. Plasmas **20**, 102507 (2013).

[8] A. S. Kukushkin1, H.D. Pacher, G.W. Pacher, V. Kotov, R.A. Pitts and D. Reiter, Nucl. Fusion **53,** 123024 (2013).

[9] P. Stiab, J. Nucl. Mater. **111-112**, 109 (1982).

[10] S.-I. Itoh and K. Itoh, Plasma Phys. Control. Fusion **36,** 1845 (1994).

[11] G. F. Counsell, J.W. Connor, S.K. Erents, A.R. Field, S.J. Fielding, B. La Bombard and K.M. Morel, J. Nucl. Mater. **266**–**269**, 91 (1999).

[12] J.-W. Ahn, G. F. Counsell, and A. Kirk, Plasma Phys. Controlled Fusion **48**, 1077 (2006).

[13] J. W. Connor, G.F. Counsell, S.K. Erents, S.J. Fielding, B. LaBombard and K. Morel, Nucl. Fusion **39**, 169 (1999).

[14] R. Maingi, C. E. Bush, R. Kaita, H. W. Kugel, A. L. Roquemore, S. F. Paul, V. A. Soukhanovskii, and NSTX Team, J. Nucl. Mater. **363–365**,196 (2007).

[15] T. Eich, B. Sieglin, A. Scarabosio, W. Fundamenski, R. J. Goldston, A. Herrmann, and ASDEX Upgrade Team, Phys. Rev. Lett. **107**, 215001 (2011).

[16] B. LaBombard, J. L. Terry, J. W. Hughes, D. Brunner, J. Payne, M. L. Reinke, I. Cziegler, R. Granetz, M. Greenwald, I. H. Hutchinson, J. Irby, Y. Lin, B. Lipschultz, Y. Ma, E. S. Marmar, W. L. Rowan, N. Tsujii, G. Wallace, D. G. Whyte, S. Wolfe, S. Wukitch, G. Wurden, and Alcator C-Mod Team, Phys. Plasmas **18**, 056104 (2011).

[17] T. K. Gray, J.M. Canik, R. Maingi, A.G. McLean, J-W. Ahn, M.A. Jaworkski, R. Kaita, M. Ono, S.F. Paul and the NSTX Team, Nucl. Fusion **54**, 023001 (2014).

[18] C. J. Lasnier, M. A. Makowski, J. A. Boedo, S. L. Allen, N. H. Brooks, D. N. Hill, A. W. Leonard, J. G. Watkins, and W. P. West, J. Nucl. Mater. **415**, S353 (2011).

[19] J. R. Harrison, G.M. Fishpool, A. Kirk, J. Nucl. Mater. **438**, S375 (2013).

[20] L. Wang, H.Y. Guo, G.S. Xu, S.C. Liu, K.F. Gan, H.Q. Wang, X.Z. Gong, Y. Liang, X.L. Zou, J.S. Hu, L. Chen, J.C. Xu, J.B. Liu, N. Yan, W. Zhang, R. Chen, L.M. Shao, S. Ding, G.H. Hu, W. Feng, N. Zhao, L.Y. Xiang, Y.L. Liu, Y.L. Li, C.F. Sang, J.Z. Sun, D.Z. Wang, H.B. Ding, G.N. Luo, J.L. Chen, X. Gao, L.Q. Hu, B.N. Wan, J. Li and the EAST Team, Nucl. Fusion **54**, 114002 (2014).

[21] W. Fundamenski, T. Eich, S. Devaux, S. Jachmich, M. Jakubowski, H. Thomsen, G. Arnoux, F. Militello, E. Havlickova, D. Moulton, S. Brezinsek, G. Maddison, K. McCormick, A. Huber and JET EFDA Contributors, Nucl. Fusion **51** 083028 (2011).

[22] T. Eich, A.W. Leonard, R.A. Pitts, W. Fundamenski, R.J. Goldston, T.K. Gray, A. Herrmann, A. Kirk, A. Kallenbach, O. Kardaun, A.S. Kukushkin, B. LaBombard, R. Maingi, M.A. Makowski, A. Scarabosio, B. Sieglin, J. Terry, A. Thornton and ASDEX Upgrade Team and JET EFDA Contributors Nucl. Fusion **53,** 093031 (2013).

[23] G. Arnoux, T. Farley, C. Silva, S. Devaux, M. Firdaouss, D. Frigione, R. J. Goldston, J. Gunn, J. Horacek, S. Jachmich, P.J. Lomas, S. Marsen, G.F. Matthews, R.A. Pitts, M. Stamp, P. Stangeby and JET-EFDA contributors, Nucl. Fusion **53**, 073016 (2013).

[24] C. Silva, G. Arnoux, S. Devaux, D. Frigione, M. Groth, J. Horacek1, P.J. Lomas, S. Marsen, G. Matthews, L. Meneses, R.A. Pitts and JET-EFDA Contributors, Nucl. Fusion **54**, 083022 (2014).

[25] P. Simon, M. Ramisch, A. A. Beletskii, A. Dinklage, M. Endler, S. Marsen, B. Nold, U. Stroth, P. Tamain and R Wilcox, Plasma Phys. Control. Fusion **56**, 095015 (2014).

[26] Y. Corre, J.P. Gunn, M. Firdaouss, S. Carpentier, M. Chantant, L. Colas, A. Ekedahl, J.-L. Gardarein, M. Lipa, T. Loarer, X. Courtois, D. Guilhem and F. Saint-Laurent, Nucl. Fusion **54**, 013013 (2014).

[27] X. Q. Xu, R. H. Cohen, T. D. Rognlien, and J. R. Myra, Phys. Plasmas **7**, 1951 (2000).

[28] X. Q. Xu, W. M. Nevins, T. D. Rognlien, R. H. Bulmer, M. Greenwald, A. Mahdavi, L. D. Pearlstein and P. Snyder, Phys. Plasmas **10**, 1773 (2003).

[29] R. H. Cohen, B. LaBombard, D. D. Ryutov, J. L. Terry, M. V. Umansky, X. Q. Xu and S. Zweben, Nucl. Fusion **47**, 612 (2007).

[30] B. I. Cohen, M. V. Umansky, W. M. Nevins, M. A. Makowski, J. A. Boedo, D. L. Rudakov, G. R. McKee, Z. Yan, and R. J. Groebner, Phys. Plasmas **20**, 055906 (2013).

[31] B. N. Rogers, J. F. Drake and A. Zeiler, Phys. Rev. Lett. **81** (1998) 4396.

[32] B. Scott, Phys. Plasmas **7**, 1845 (2000); and Plasma Phys. Control. Fusion **49**, S25 (2007).

[33] K. Hallatschek, Plasma Phys. Control. Fusion **49**, B137 (2007).

[34] P. Beyer, S. Benkadda, G. Fuhr-Chaudier, X. Garbet, Ph. Ghendrih, Y. Sarazin, Plasma Phys. Control. Fusion **49**, 507 (2007).

[35] V. Naulin, A. Kendl, O. E. Garcia, A. H. Nielsen and J. Juul Rasmussen, Phys. Plasmas **12**, 052515 (2005).

[36] P. Guzdar, R. Kleva, R. Groebner, and P. Gohil, Phys. Plasmas **11**, 1109 (2004).

[37] P. Ricci and B. N. Rogers, Phys. Plasmas **20**, 010702 (2013).

[38] O. E. Garcia, V. Naulin, A. H. Nielsen, and J. J. Rasmussen, Phys. Plasmas **12**, 062309 (2005).

[39] D. A. Russell, J. R. Myra and D. A. D'Ippolito, Phys. Plasmas **16**, 122304 (2009).

[40] S. I. Krasheninnikov, D. A. D'Ippolito and J. R. Myra, J. Plasma Phys. **74**, 679 (2008).

[41] D. A. D'Ippolito, J. R. Myra and S. J. Zweben, Phys. Plasmas **18**, 060501 (2011).

[42] J. R. Myra, D. A. Russell, D. A. D'Ippolito, J.-W. Ahn, R. Maingi, R. J. Maqueda, D. P. Lundberg, D. P. Stotler, S. J. Zweben, J. Boedo, M. Umansky, and NSTX Team, Phys. Plasmas **18**, 012305 (2011).

[43] D. A. Russell, D. A. D'Ippolito, J. R. Myra, B. LaBombard, J. L. Terry and S. J. Zweben, Phys. Plasmas **19**, 082311 (2012).

[44] F. Militello, V. Naulin and A. H. Nielsen, Plasma Phys. Control. Fusion **55**, 074010 (2013).

[45] D. A. Russell, D. A. D'Ippolito, J. R. Myra, J. M. Canik, T.K. Gray and S. J. Zweben, 25th IAEA Fusion Energy Conference, Saint Petersburg, Russia, October 13 - 18, 2014, paper IAEA-CN-221/TH/P6-52.

[46] F. D. Halpern, P. Ricci, B. Labit, I. Furno, S. Jolliet, J. Loizu, A. Mosetto, G. Arnoux, J. P. Gunn, J. Horacek, M. Kocan, B. LaBombard, C. Silva, and JET-EFDA, Nucl. Fusion **53**, 122001, (2013).

[47] F. D. Halpern, P. Ricci, S. Jolliet, J. Loizu and A. Mosetto, Nucl. Fusion **54**, 043003 (2014).

[48] J. Loizu, P. Ricci, F. D. Halpern, S. Jolliet and A. Mosetto, Nucl. Fusion **54**, 083033 (2014).

[49] R. J. Goldston, Nucl. Fusion **52**, 013009 (2012).

[50] C. S. Chang and S. Ku, Phys. Plasmas **11**, 2649 (2004).

[51] A.Y. Pankin, G.Y. Park, J. Cummings, C.S. Chang, G. Bateman, D. Bunner, R.J. Groebner, J.W. Hughes, B. LaBombard, J.L. Terry, A.H. Kritz, S. Ku, T. Rafiq, and P.B. Snyder, Problems of Atomic Science and Technology, Series: Plasma Physics **17**, 8 (2011).

[52] S. Ku, C.S. Chang and P.H. Diamond, Nucl. Fusion **49**, 115021 (2009).

[53] C. S. Chang, J. A. Boedo, R. Hager, S.-H. Ku, J. Lang, R. Maingi, D. Stotler, S. Zweben, and S. Parker, 25th IAEA Fusion Energy Conference, Saint Petersburg, Russia, October 13 - 18, 2014, paper IAEA-CN-221/TH/2-3.

[54] Peter C. Stangeby, *The Plasma Boundary of Magnetic Fusion Devices*, (Institute of Physics Publishing, Bristol and Philadelphia, PA, 2000).

[55] J. R. Myra, D.A. D'Ippolito, X.Q. Xu and R.H. Cohen, Phys. Plasmas **7**, 4622 (2000).

[56] W. Kerner, O. Pogutse and R. Van der Linden, Plasma Phys. Control. Fusion **39**, 757 (1997).

[57] F. D. Halpern, S. Jolliet, J. Loizu, A. Mosetto, and P. Ricci, Phys. Plasmas **20**, 052306 (2013).

[58] F.W. Perkins and D.L. Jassby, Phys. Fluids **14**, 102 (1971).

[59] P. H. Diamond and Y.-B. Kim, Phys. Fluids B **3**, 1626 (1991).

[60] K. H. Burrell, Phys. Plasmas **4**, 1499 (1997).

[61] K. Miki, P. H. Diamond, O. D. Gurcan, G. R. Tynan, T.Estrada, L. Schmitz, and G. S. Xu, Phys. Plasmas **19**, 092306 (2012) ; and refs. therein

[62] G. S. Xu, B. N. Wan, H. Q. Wang, H.Y. Guo, H. L. Zhao, A. D. Liu, V. Naulin, P. H. Diamond, G. R. Tynan, M. Xu, R. Chen, M. Jiang, P. Liu, N. Yan, W. Zhang, L. Wang, S. C. Liu, and S.Y. Ding, Phys. Rev. Lett. **107**, 125001 (2011).

[63] L. Schmitz, L. Zeng, T. L. Rhodes, J. C. Hillesheim, E. J. Doyle, R. J. Groebner, W.A. Peebles, K. H. Burrell, and G. Wang, Phys. Rev. Lett. **108**, 155002 (2012).

[64] G.R. Tynan, M. Xu, P.H. Diamond, J.A. Boedo, I. Cziegler, N. Fedorczak, P. Manz, K. Miki, S. Thakur, L. Schmitz, et al., Nucl. Fusion **53**, 073053 (2013).

[65] M. Ono, S.M. Kaye, Y.-K.M. Peng, G. Barnes, W. Blanchard, M.D. Carter, J. Chrzanowski, L. Dudek, R. Ewig, D. Gates, et al., Nucl. Fusion **40**, 557 (2000).

[66] S. J. Zweben, R. J. Maqueda, D. P. Stotler, A. Keesee, J. Boedo, C. E. Bush, S. M. Kaye, B. LeBlanc, J. L. Lowrance, V. J. Mastrocola, R. Maingi, N. Nishino, G. Renda, D. W. Swain, J. B.Wilgen and the NSTX Team, Nucl. Fusion **44**, 134 (2004).

[67] K. H. Finken, T. Denner and G. Mank, Nucl. Fusion **40**, 339 (2000).

[68] B. LaBombard, J. W. Hughes, N. Smick, A. Graf, K. Marr, R. McDermott, M. Reinke, M. Greenwald, B. Lipschultz, J. L. Terry, D. G. Whyte, S. J. Zweben, and Alcator C-Mod Team, Phys. Plasmas **15**, 056106 (2008).

[69] M. A. Makowski, D. Elder, T. K. Gray, B. LaBombard, C. J. Lasnier, A. W. Leonard, R. Maingi, T. H. Osborne, P. C. Stangeby, J. L. Terry, and J. Watkins, Phys. Plasmas **19**, 056122 (2012).

[70] R. J. Goldston and T. Eich, 24th IAEA Fusion Energy Conference, October 8-13, 2012, San Diego, California, paper 251-TH/P4-19.

[71] R.J. Goldston, J. Nucl. Mater. (2015) in press, http://dx.doi.org/10.1016/j.jnucmat.2014.10.080

[72] P. Ricci, B. N. Rogers and S. Brunner, Phys. Rev. Lett. **100**, 225002 (2008).